A Comparison between the Hoskins-Bretherton Model of Frontogenesis and the Analysis of an Intense Surface Frontal Zone

WILLIAM BLUMEN

Department of Astro-Geophysics, University of Colorado, Boulder 80309

(Manuscript received 18 June 1979, in final form 17 August 1979)

ABSTRACT

The Hoskins-Bretherton model of frontogenesis employed here represents the counterpart of the two-dimensional Eady problem expressed in geostrophic coordinate space. The fundamental characteristics of the model solution are shown to be derivable from the properties of the nonlinear one-dimensional advection equation and the linearized Eady problem. Detailed comparisons are made between the predictions of this model and the analysis of an intense frontal zone presented by Sanders. Qualitative agreement is found in details of the horizontal wind field and potential temperature distributions. The major discrepancy occurs in the vertical velocity field: the most intense vertical velocities occur at midlevel in the model and are significantly smaller in magnitude than the rising narrow jet above the analyzed zone of maximum cyclonic relative vorticity. The presence of this jet is responsible for the most significant frontogenetical properties of the front associated with vertical tilting of potential isotherms and isopleths of the horizontal velocity component parallel to the frontal zone. In contrast, ageostrophic convergence and horizontal distortion of potential isotherms make the largest contribution to frontogenesis in the model.

Ekman-layer pumping is introduced into the model to simulate the vertical velocity jet. Yet this feature is not sufficient to increase the contribution of vertical tilting to frontogenesis because the vertical gradients of potential temperature and geostrophic velocity are weaker in this case.

Trajectories of the air motion tend to show the pattern of upgliding warm air ahead of the frontal zone with relatively stagnant cold air to the rear. In general, the model is able to provide qualitative agreement with gross features of this frontal situation. Discrepancies seem to be associated with the absence of a realistic boundary layer formulation and mesoscale mixing processes in the model.

1. Introduction

Atmospheric fronts have been studied from many different vantages, both theoretical and observational. Most studies have been motivated by intrinsic interest in the frontal phenomenon itself. Less attention has been paid to the role of fronts as a coupling agent between relatively large-scale energy bearing baroclinic modes and small-scale dissipative modes. Recent work by Andrews and Hoskins (1978) and by Gall *et al.* (1979), for example, suggest that the energy spectrum of atmospheric motions for zonal wavenumbers $n \geq 10$ may actually be indicative of energy transfer processes associated with frontal formation rather than inertial energy transfer associated with quasi-geostrophic turbulence (Charney, 1971).

The distinction between each of these characteristic energy spectra would be difficult to distinguish from observations, since the former spectrum tends to a $-8/3$ spectral decay while the latter is characterized by a -3 slope. The energy spectrum found by Andrews and Hoskins was based on a two-dimensional (horizontal and vertical) inviscid model of frontogenesis developed earlier by Hoskins and Bretherton (1972). Although the model is limited in scope, because dissipative processes are neglected and because the flow conserves uniform potential vorticity, the model does describe the large-scale forcing of the frontogenetical process by unstable baroclinic wave development. As a consequence, the physical process of energy transfer down the spectrum is a by-product of the model. As noted in Section 2, the rate of transfer across the spectrum approaches n^{-1} as the $-8/3$ spectral slope develops. However, this model merits closer examination if its predictions are to provide useful insights into the structure and energetics of atmospheric motions.

The purpose of the present investigation is to provide a detailed comparison between an actual synoptic situation examined by Sanders (1955) and the predictions of the Hoskins and Bretherton model of frontogenesis. This comparison should be viewed with some care, since only one case study is used and because Hoskins (1976) and Hoskins and West (1979) have since provided significant improvements to the basic model. However, it is possible to present very detailed calculations of the

0022-4928/80/010064-14$07.50

solution of the Hoskins and Bretherton model equations in physical space, rather than in the transformed geostrophic coordinates used in the model extensions. This advantage proves extremely useful in making one-to-one comparisons between the model predictions and the analysis of the observed event.

2. Theory

The basic model solution employed in this study represents the counterpart of the two-dimensional Eady problem expressed in nondimensional coordinate space defined by

$$X = x + \mathrm{Ro}\, v_g, \quad Z = z, \quad T = t. \tag{1}$$

Here (x,z) are physical space coordinates directed eastward and upward respectively, $v_g(x,z,t)$ is the northward directed geostrophic velocity, t represents time; the Rossby number $\mathrm{Ro} \equiv U/f_0L$ is defined in terms of a characteristic amplitude U of the basic geostrophic zonal flow $u_g = \bar{u}(z)$, the constant Coriolis parameter f_0, and the characteristic quarter-wavelength L of the initial disturbance. For the present, the magnitude of Ro will not be specified.

The details of the model development have been reported by Hoskins and Bretherton (1972) and Hoskins (1975, 1976). Only a brief resume of the theory will be presented here to acquaint the reader with the essential background relevant to the present investigation. Hereafter, the "HB model" will refer to the Eady problem in coordinate space defined by (1) that is associated with the authors cited above.

The nondimensional geostrophic velocity for this model may be expressed as

$$v_g = kA(Z')\cos[kX' + \delta(Z')]e^{\sigma T}, \tag{2}$$

where $X' = X - \frac{1}{2}T, Z' = Z - \frac{1}{2}, k$ denotes the X' wavenumber, σ is the unstable growth rate of the disturbance, $A(Z')$ represents the amplitude of the streamfunction Φ ($v_g = \Phi_{X'}$), and $\delta(Z')$ is a phase factor. The fluid is bounded by rigid lids at $Z = 0, 1$ ($Z' = \pm\frac{1}{2}$), where the vertical velocity vanishes. The disturbance motion is viewed from a coordinate frame (X',Z',T) that moves with the basic flow at midlevel, $\bar{u} = \frac{1}{2}$; in this coordinate system, the phase of the wave disturbance is stationary at all levels Z'.

Andrews and Hoskins (1978) have shown that v_g may be represented in physical space ($x' = x - \frac{1}{2}t$, $z' = z - \frac{1}{2}, t$) as a Fourier series. In particular, the solution at the lower boundary may be expressed as (Blumen, 1979)

$$v_g(x', -\tfrac{1}{2}, t) = 2/\mathrm{Ro}\, k \sum_{n=1}^{\infty} v_n(t)\sin[n(kx' + \delta + \pi/2)], \tag{3}$$

where

$$v_n(t) = n^{-1}J_n(n\mathrm{Ro}\, k^2Ae^{\sigma t}) \tag{4}$$

and J_n denotes the Bessel function of order n. Similar expressions hold for $v_g(x',z',t)$ and for other flow variables.

The ageostrophic flow field may be determined once the geostrophic field is found. In particular, the vertical velocity w may be determined from the equation that expresses conservation of potential temperature and the horizontal ageostrophic component $u(x',z',t)$ is given by

$$u = -\mathrm{Ro}\left[\frac{\partial}{\partial t} + (u_g + u)\frac{\partial}{\partial x'} + w\frac{\partial}{\partial z'}\right]v_g = -\mathrm{Ro}\left(\frac{\partial}{\partial T} + u_g\frac{\partial}{\partial X'} + w\frac{\partial}{\partial Z'}\right)v_g. \tag{5}$$

Detailed calculations of u and w have been carried out by Blumen (1979).

The relationship that exists between (3) and (4) and the solution of the one-dimensional advection equation (e.g., Platzman, 1964) provides a ready interpretation of some physical aspects of the HB model; the relationship to the Eady problem completes the picture. The finite-amplitude, one-dimensional flow of a perfect gas, for example, is governed by the advection equation

$$\partial\phi/\partial\tau + \phi\partial\phi/\partial\chi = 0, \tag{6}$$

where ϕ is a velocity variable, χ the spatial coordinate, and τ time. The spectral solution of (6), associated with an initial condition $\phi(\chi,\tau_i)$, is given by

$$\phi(\chi,\tau) = -2\sum_{n=1}^{\infty}(n\tau)^{-1}J_n(n\tau)\sin n\chi. \tag{7}$$

This solution is credited to Fubini-Ghiron (1935) but, according to Benton and Platzman (1972), has been rediscovered by workers in several different fields. Platzman (1964) has provided a clear exposition of the solution (7) and some of its properties.

The properties of the advection equation (6) may be exploited by means of the transformation

$$\left.\begin{aligned}\tau &= \mathrm{Ro}\, k^2A\exp(\sigma t)\\ \chi &= kx' + \delta + \pi/2\\ \phi &= -\mathrm{Ro}\, kv_g/\tau\end{aligned}\right\}. \tag{8}$$

Then (3) and (4) transform into (7) and ϕ satisfies (6). Since $v_g(X', -\frac{1}{2}, T)$ is stationary in a coordinate frame moving at the midlevel translation speed, not the ground level speed, it is necessary to redefine X' or x' to effect a one-to-one correspondence between the HB model solution and the solution of the advection equation. This is accomplished by reinterpreting x' to be $x' + \frac{1}{2}t$. This translation along the x' axis does not affect the physical properties of interest in this section. The variable ϕ still satisfies (6), but now $\chi = k(x' + \frac{1}{2}t) + \delta + \pi/2$.

Platzman used (6) to show that $-\phi$ develops an infinite slope in a finite time, a result later established by Andrews and Hoskins from (3) and (4). The critical time of occurrence is $\tau_c = 1$. In terms of the HB model, $\tau_c = 1$ corresponds to the formation of an infinity in positive (cyclonic) relative vorticity $\partial v_g/\partial x'$ in physical space at time $t_c = -\sigma^{-1} \ln \mathrm{Ro}\, k^2 A$. Some typical values of t_c have been presented by Blumen (1979). Moreover, Platzman showed that as $t \to t_c$, and n large, the energy spectrum has the distribution $n^{-8/3}$ and the rate of energy transfer across the spectrum is proportional to n^{-1}. The former result was also confirmed by Andrews and Hoskins.

The physical picture of frontogenesis depicted by the HB model is in essence described by (6). Hoskins and Bretherton (1972) derived an approximate version of (6) which applies when $t \to t_c$.

In terms of (6), ϕ is propagated along the χ axis with speed ϕ such that the wave crest of ϕ is propagated in the positive direction and the wave trough is propagated in the negative direction. In view of (8), the wave crest of v_g is propagated toward negative x and the trough of v_g toward positive x. This process increases the cyclonic shear and lessens the anticyclonic shear. At the same time, exponential growth of the wave amplitude occurs due to baroclinic instability of the basic shear flow. This latter feature accelerates the advection process as evident from the appearance of $\tau \propto \exp\sigma t$ as the time scale. The time development of v_g, given by (3) and (4), that has been presented by Blumen (1979, Fig. 1) clearly shows these features. This characteristic pattern of wave steepening, based on the nature of the coordinate transformation (1), has also been presented by Hoskins (1975).[1] Furthermore, the amplitude $|A|$ has maxima on the boundaries, so that $\partial v/\partial x$ first becomes infinite on these boundaries. Thereafter, for $t > t_c$, transformation (1) is invalid because the solution is multi-valued. However, before this occurs viscosity and small-scale mixing would be expected to become important and to alter the frontogenetical processes.

Other details of the theory will be examined in conjunction with analyzed frontal properties.

3. Comparison between theory and observation

Sanders (1955) presented a highly detailed analysis of an intense cold front that moved southward through a dense observational network in the south central United States during the period 17–18 April 1953. Noteworthy features revealed by this analysis are the large gradients of both potential temperature and wind, which achieve maxima at ground level, and the marked increase in the horizontal width of the frontal zone with altitude. For example, in three different cross sections through the front, the zone width increased by a factor of 5–10 between an altitude of 300 to 900 m above the surface, with complementary decreases in the gradients of potential temperature and wind parallel to the front over the same altitude range. These features are qualitatively similar to features in the meteorological fields predicted by the HB model that have been presented by Blumen (1979).

A more detailed comparison between the HB model predictions and Sanders' frontal analysis was undertaken to further examine the extent to which the model provides a realistic description of a surface-type frontal zone. However, there is one significant difference between the model solution and the meteorological situation: the observed frontal zone *appears* to have a relatively uniform intensity, with an approximate balance between its frontogenetical and frontolytical properties. In contrast, the HB model exhibits predominantly frontogenetical properties with the ultimate development of an infinity in cyclonic relative vorticity in a finite time. Nonetheless, the HB model solution does exhibit sufficient similarities with the frontal analysis to warrant closer examination.

Reference to the large number of figures in Sanders' paper and those presented here will be facilitated by introduction of the following nomenclature: S(N) and B(N) refer, respectively, to Sanders and Blumen, where N designates the figure number. All the HB model solutions in physical space, in a coordinate system (x',z',t) moving with the midlevel zonal flow, are based on a highly accurate approximation presented by Blumen. All dependent model variables were evaluated from the analytical solution at intervals of 5 km in the horizontal and 250 m in the vertical. The calculated fields represent the solution 6 h before the discontinuity forms, in terms of the characteristic parameter values used. These values are

$$L = N_0 H/f_0 \approx 1000 \text{ km},$$

$$\mathrm{Ro} = U_0/f_0 L = 0.2,$$

where L is the characteristic horizontal scale of the initial disturbance (quarter wavelength), Ro the Rossby number associated with this disturbance, N_0 is the constant Brunt-Väisälä frequency, H represents the fluid depth, U_0 the amplitude of the basic zonal flow, and f_0 the constant Coriolis parameter. These values are more or less characteristic of large-scale stably stratified midlatitude flow if H is considered to be the depth of the troposphere. Other parameter values, such as the unstable growth rate, etc., have been presented by Blumen.

[1] In fact, the advection equation (6), with ϕ given by (8), is nothing more than a restatement of coordinate transformation (1).

a. Features of the flow

Large-scale features of the synoptic pattern on 17–18 April 1953 appear in S(1)–S(6). We shall be concerned here with the mesoscale features in the vicinity of the frontal boundaries. In particular, these features are presented by Sanders in a two-dimensional cross section, along a line EN, extending approximately from southern Saskatchewan to Kansas. The horizontal scale, unspecified in his diagrams, is represented by 100 km increments between letters along the abscissa of S(9). The region of interest is primarily confined between 1000 and 700 mb in the vertical. For practical purposes, each increment of 100 mb corresponds to a depth of 1 km. The sloping lower boundary, over the Great Plains, has not been taken into account in the model calculations.

The location of the frontal zone above the lower boundary was depicted by soundings presented in S(8). The fields of potential temperature, horizontal wind parallel to the front, vertical velocity and horizontal divergence appear in S(9) and S(10), with the frontal zone boundaries shown by thick solid lines. The features of note are (i) the relatively large gradients of potential temperature and horizontal wind across the frontal zone, pointed out earlier; (ii) large values of horizontal convergence, with values in excess of -10^{-4} s^{-1} in the lowest kilometer of the frontal zone; and (iii) a "jet of extremely intense rising motion immediately above the position of the zone at the ground." This latter feature (iii) is shown to be one of the principal discrepancies between the observed and model features of the frontal situation.

As noted above, the HB model cannot be expected to provide a detailed simulation of the relative small-scale features analyzed by Sanders. Moreover, the frontogenetical properties of the HB model, as described in Section 2, are relatively insensitive to the initial conditions. Consequently, the parameter values associated with the frontal features displayed by Blumen (1979, Figs. 4 and 5) have been adopted for present use. The model predictions at $t = 5.25$ ($t = t_c - 6$ h) are used for comparison with Sanders' analyses.

The vertical temperature distributions predicted by the model are shown in B(1). In this Boussinesq system, the pressure coordinate $p^{-\kappa}$ (κ denotes the ratio of the gas constant to the specific heat at constant pressure) is directly proportional to height z, which is used in place of pressure here. The temperature distributions exhibit inversions and isothermal layers in the cold air region behind the position of maximum cyclonic relative vorticity at ground level; ahead of this position there is a region where the lapse rate is adiabatic in the lowest layer [see also B(3)]. The absence of nonadiabatic thermal interaction between the overlying atmosphere and the ground presumably accounts for the absence of lower boundaries for these temperature inversions. Hereafter, the sloping boundary defined by the top of the inversion or isothermal layer in B(1) will be referred to as the "front." However, the following two figures show that the frontal zone

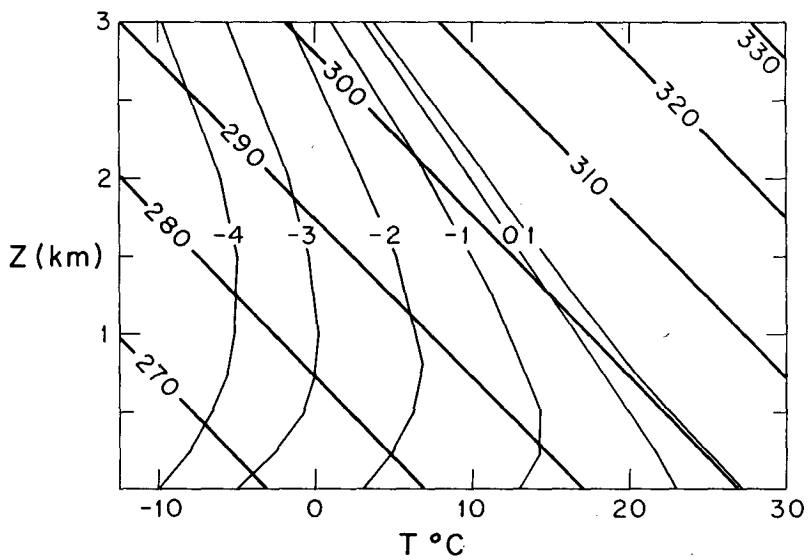

FIG. 1. Temperature T as a function of height z above the ground. The label on each curve, in units of 100 km, denotes the point where the ground-level temperature is located relative to the point of maximum cyclonic relative vorticity at the ground. The sloping straight lines are adiabats labeled in Kelvins.

is not well-defined by the HB model predictions: the "front," the axis of maximum cyclonic relative vorticity, and the axis of maximum horizontal temperature gradient are not coincident as in Sanders' analyses [S(8), S(9) and Table 1].

The geostrophic wind parallel to the front is shown in B(2). The wind maxima, over 50 m s^{-1}, are much larger than observed values. However, the cyclonic shear in the vicinity of the front ($\sim 4.5 \times 10^{-4}$ s^{-1}) is less than the value reported by Sanders. In the observed case the transition zone extends over a width of ~25 km compared to a somewhat nebulous dimension of 100–200 km in the model. At a later time, the model transition zone would be smaller, but the variable quantities would become unusually excessive close to the critical time of the model's breakdown.

The field of potential temperature in B(3) reflects a transition zone between warm and cold air but, as in B(1), is not well defined. The horizontal divergence field in B(4) shows qualitative similarities to the field in S(10), although the maximum value of convergence in the frontal zone is smaller by a factor of 4. The notable jet of rising air in S(10) does not appear in B(4). Rather, the model predicts a maximum vertical velocity at midlevel (5 km) of $\sim 4 \times 10^{-2}$ ms^{-1} (Blumen, 1979, Fig. 4). This feature of the model reflects the "two-layer" characteristic of the Eady model, pointed out by Bretherton (1966), which is associated with maximum conversion of potential into kinetic energy to sustain the unstable growth of the disturbance. The observed low-level jet, in excess of 25×10^{-2} m s^{-1}, appears to be associated with boundary layer convergence in the vicinity of maximum cyclonic relative vorticity (see Section 4 and the Appendix). However, frictional retardation of the cold air at the ground, leading to overturning associated with static instability, may be responsible for the appearance of this jet. Elsewhere the vertical velocities are relatively weak with subsiding motions in the anticyclone behind the front. This latter feature is captured by the model.

b. Frontogenesis in the potential temperature field

Sanders examined frontogenetical and frontolytical effects by evaluating some terms in the equation for the time rate of change of the potential temperature gradient $\partial\theta/\partial x'$ following the motion (Miller, 1948), i.e.,

$$\frac{d}{dt}\left(\frac{\partial\theta}{\partial x'}\right) = -\mathrm{Ro}\left[\mathrm{Ro}\left(\frac{\partial u}{\partial x'}\frac{\partial\theta}{\partial x'}\right) + \frac{\partial w}{\partial x'}\left(1 + \mathrm{Ro}\,\frac{\partial\theta}{\partial z'}\right) + \frac{\partial v_g}{\partial x'}\right]. \quad (9)$$

Here Ro = 0.2, u is the ageostrophic component of velocity normal to the front, v_g the geostrophic velocity parallel to the front and θ refers to the potential temperature associated with the disturbance, where the constant vertical gradient of the mean value has been scaled to unity; the (x',z')

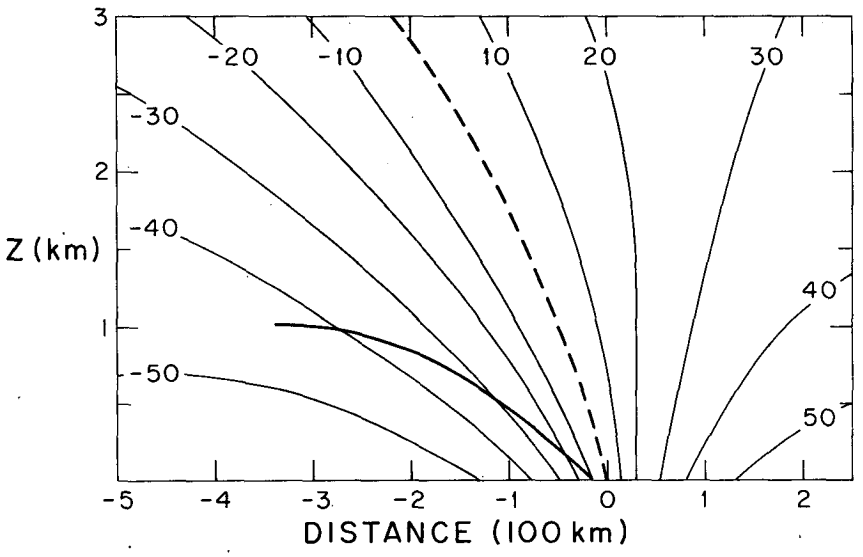

FIG. 2. Geostrophic wind v_g parallel to the front as a function of height z and distance from the point of maximum cyclonic relative vorticity at the ground. The isopleths are labeled in meters per second and v_g is positive into the paper. The solid sloping curve represents the front, determined from Fig. 1, and the dashed sloping curve is the axis of maximum cyclonic relative vorticity, $\partial v_g/\partial x'$, which is coincident with $v_g = 0$.

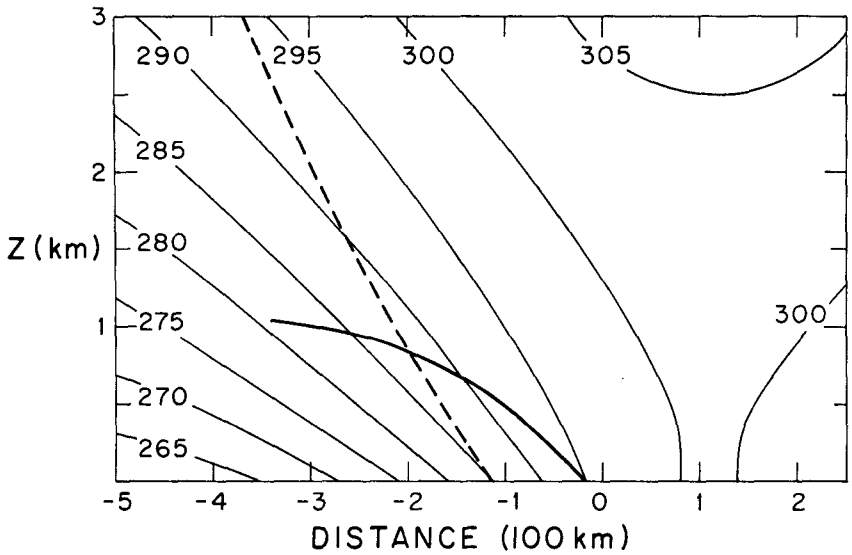

FIG. 3. Potential temperature (basic state and disturbance) distribution (K). The coordinates are as in Fig. 2. The thick solid sloping curve represents the front as in Fig. 2 but the sloping dashed curve is the axis of maximum potential temperature gradient $\partial\theta/\partial x'$.

coordinates introduced in Section 2 move with the zonal basic flow at midlevel, x' increases toward the east and z' is directed upward.

The contributions to $d(\partial\theta/\partial x')/dt$ are, respectively, 1) ageostrophic convergence that concentrates the potential temperature gradient, 2) tilting of horizontally oriented potential isotherms into an (x',z') orientation by vertical motion, and 3) distortion of the basic-state potential isotherms which are aligned along the x' axis, by the geostrophic flow v_g. This latter process, associated with baroclinic instability in the Eady model, was not evaluated by Sanders nor were nonadiabatic contributions to (9) considered. Here the former term will be evaluated but not the latter.

The convergence and vertical tilting effects in the vicinity of the front are presented respectively in S(11) and S(12); the net frontogenetical effect appears in S(13). A significant contribution to (9), associated with vertical tilting of potential iso-

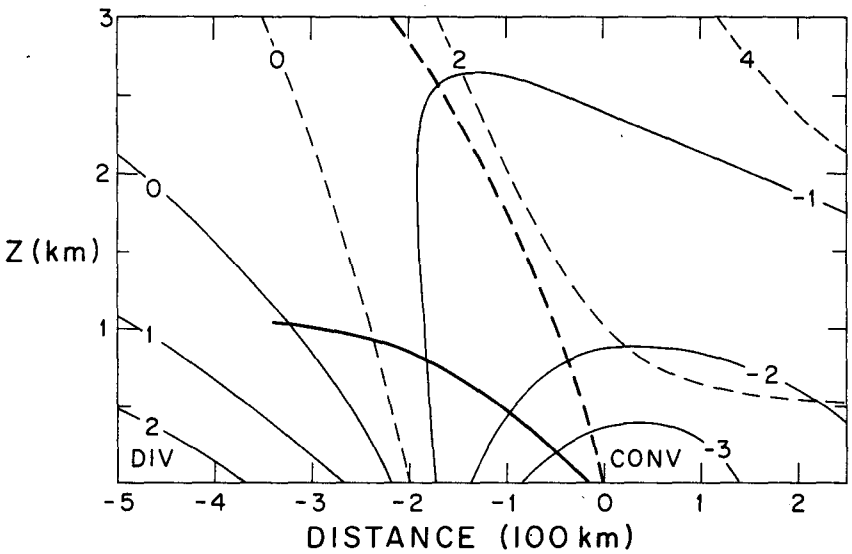

FIG. 4. Horizontal divergence (solid) in units of 10^{-5} s^{-1} and vertical velocity (dashed) in units of 10^{-2} m s^{-1}. The coordinates, thick solid and thick dashed curves are as in Fig. 2.

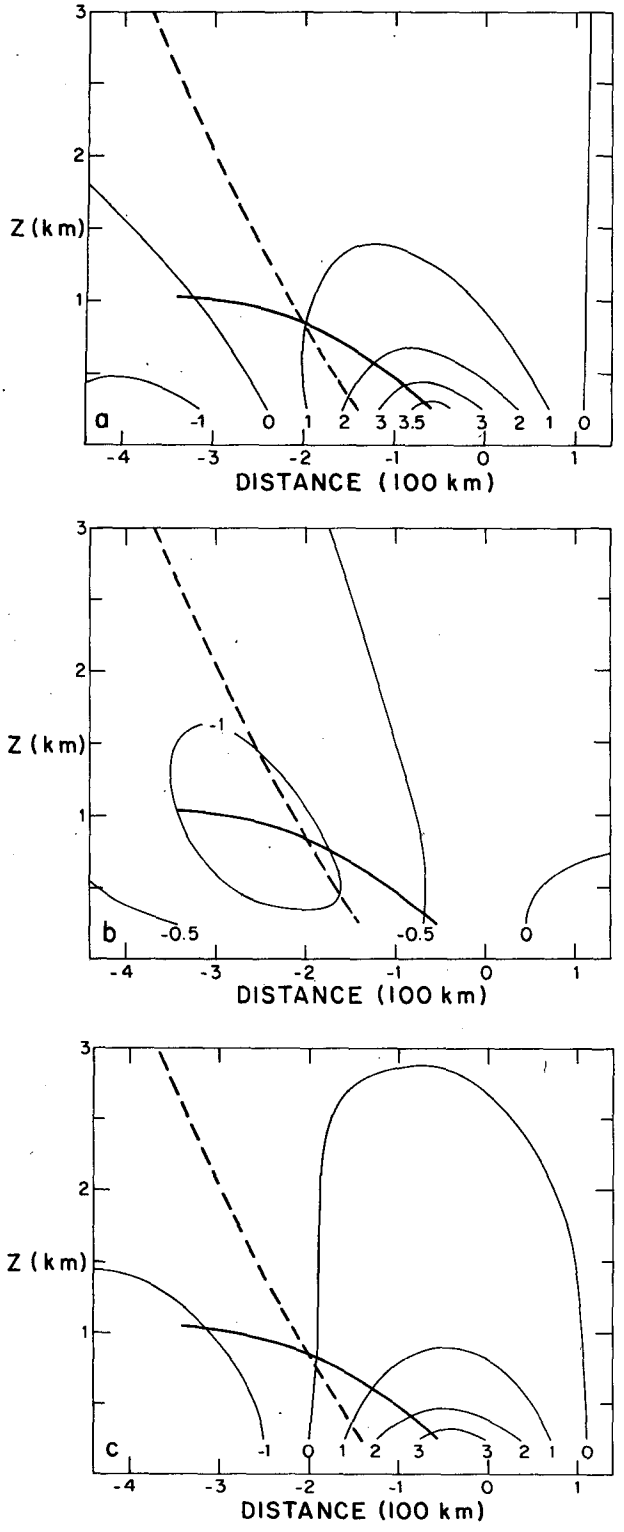

FIG. 5. Distribution of the frontogenetical effect, defined by (9), expressed in 3 h changes in the potential temperature gradient [K (100 km)$^{-1}$]: (a) $-\mathrm{Ro}^2\,\partial u/\partial x'\partial\theta/\partial x'$, (b) $-\mathrm{Ro}\,\partial w/\partial x' \times (1 + \mathrm{Ro}\,\partial\theta/\partial z')$ and (c) sum of (a) and (b). The coordinates and thick solid and dashed lines are as in Fig. 3.

therms, is produced by the rising jet of vertical motion above the surface position of the front. Behind this position, where $\partial w/\partial x' > 0$ ($-\partial w/\partial y > 0$ in Sanders' notation), the tilting process is frontolytical and ahead, where $\partial w/\partial x' < 0$, intense frontogenesis occurs with values in excess of 100 K (3 h)$^{-1}$ (100 km)$^{-1}$. Within the transition zone itself, extremely strong frontogenesis due to the convergence effect is opposed by comparable frontolysis due to the tilting effect. These contributions tend to nullify each other, leaving a residual of frontogenesis at lower altitudes and frontolysis at higher altitudes within the frontal zone. Elsewhere, all the contributions to (9) are relatively small. It is apparent that, in this type of frontal system, the frontogenetical as well as the frontolytical processes are confined to the immediate vicinity of the front within about the lowest 2–3 km above the ground.

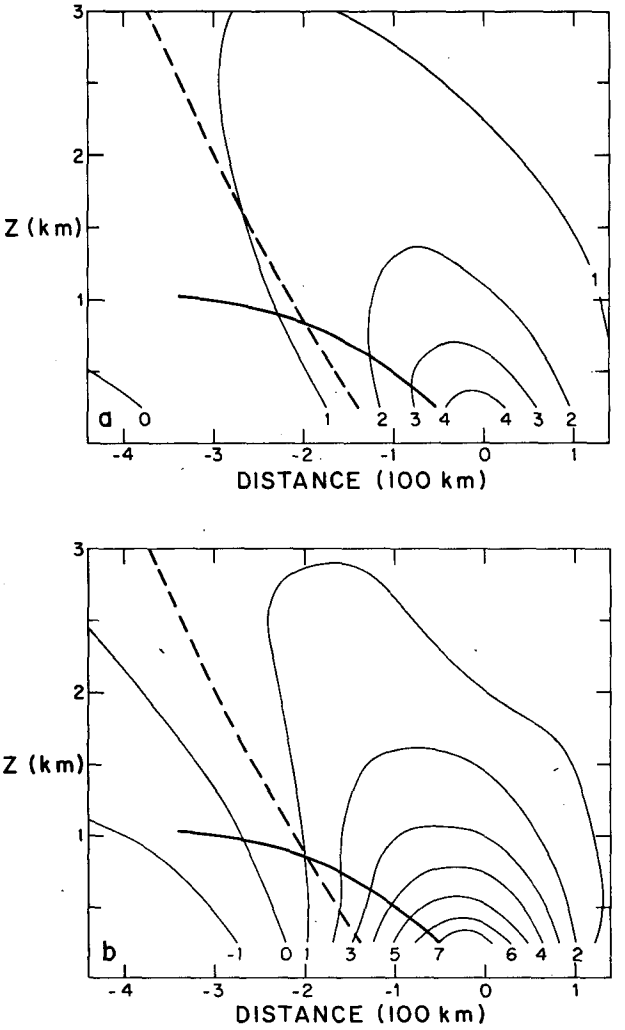

FIG. 6. Distribution of the frontogenetical effect as in Fig. 5: (a) $-\mathrm{Ro}\,\partial v_g/\partial x'$ and (b) sum of all the contributions to (9).

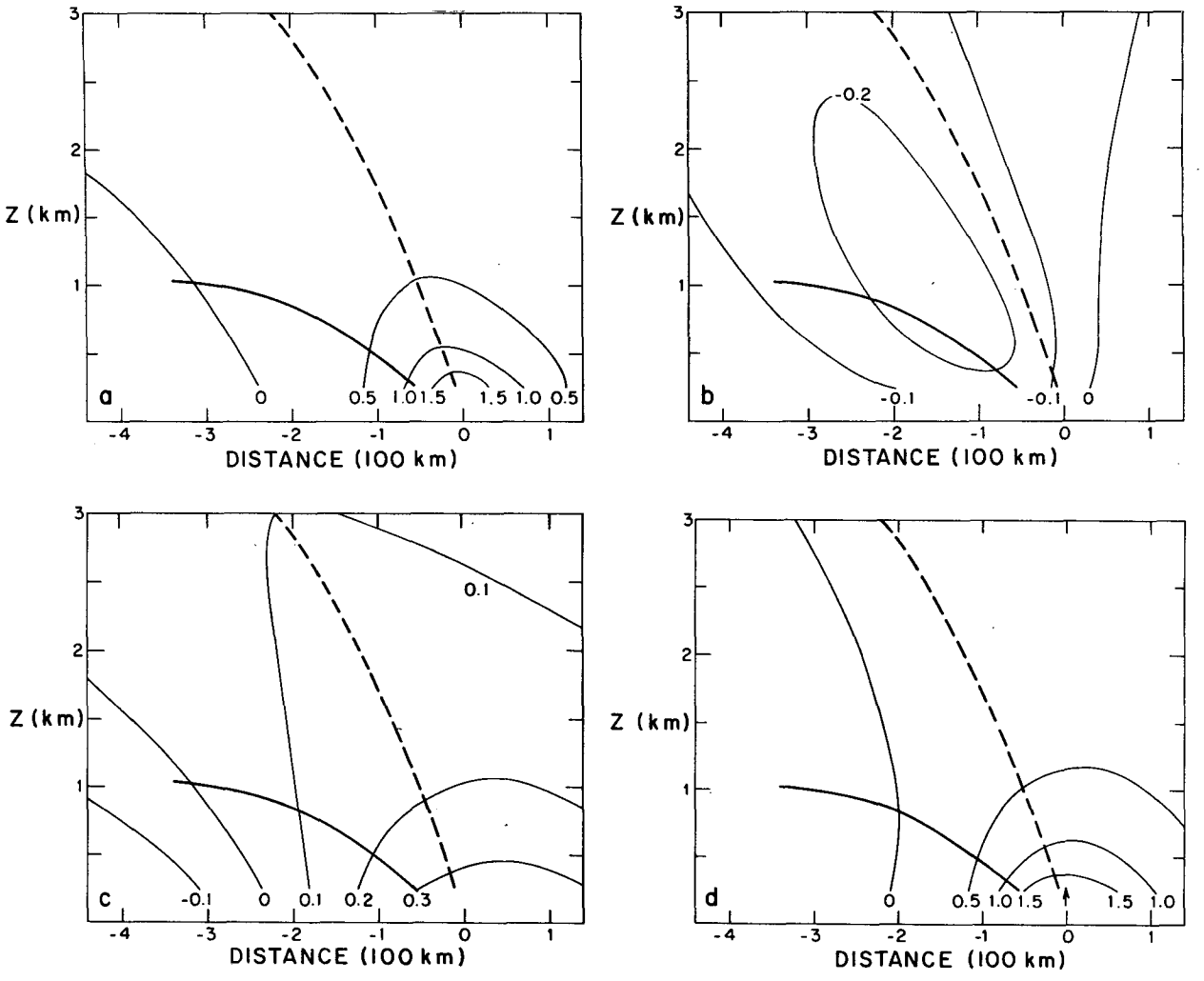

FIG. 7. Distribution of the frontogenetical effect, defined by (10), expressed in 3 h changes in the relative vorticity (10^{-4} s^{-1}): (a) $-Ro^2\ \partial u/\partial x' \partial v/\partial x'$, (b) $-Ro^2\ \partial w/\partial x' \partial v/\partial z'$, (c) $-Ro\ \partial u/\partial x'$ and (d) sum of all the contributions to (10) [(a) + (b) + (c)]. The arrow indicates a value of 2.

The evaluation of convergence and vertical tilting and their net contribution to (9), from the HB model solutions, is presented in B(5a–5c). The intense processes depicted by Sanders' analysis are not reproduced by the model: the rising jet of vertical velocity is absent and the apparent small-scale mixing processes within the frontal transition zone are omitted due to the uniform potential vorticity requirement imposed on the model. Nonetheless, some similarities are noteworthy. Convergence produces comparable values of frontogenesis at low levels ahead of the front, divergence is responsible for a lesser and more diffuse region of frontolysis in the cold anticyclone behind the front, the vertical tilting term is frontolytical in the upper portion of the front, and the primary contributions to (9) are confined to the lowest 1–2 km above the ground.

Evaluation of the third term in (9), horizontal tilting of potential isotherms, is displayed in B(6a). This term, associated with baroclinic growth of the disturbance, makes a relatively significant contribution to frontogenesis with maxima essentially occurring along the axis of maximum geostrophic shear $\partial v_g/\partial x'$ [see B(2)]. The total contribution to (9) is shown in B(6b). The contribution from the first and third terms of (9) essentially combine to produce a large contribution to frontogenesis in the lowest 2 km just ahead of the front. However, the maximum intensity is an order of magnitude smaller than the maximum in S(13), associated with vertical tilting of potential isotherms.

c. *Frontogenesis in the wind field*

The development of strong cyclonic shear of the motion directed parallel to the front was also investi-

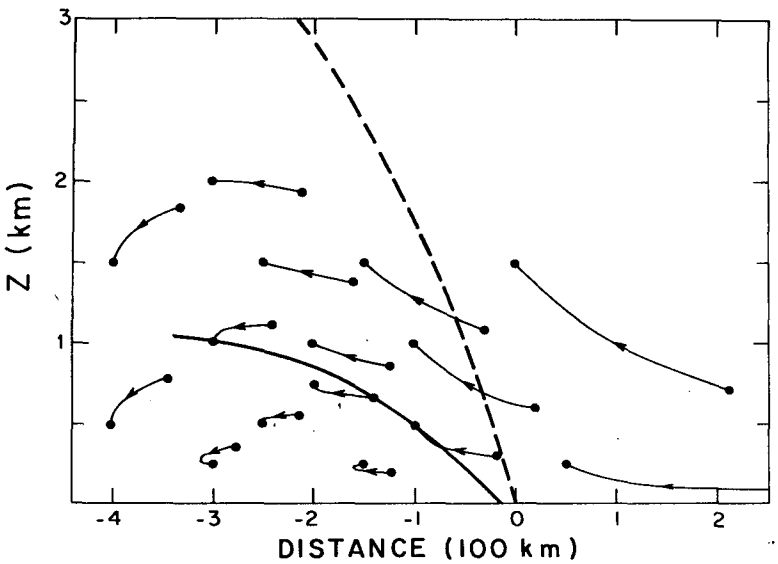

FIG. 8. Trajectories of the air motion at increments of 0.5 h for the 12 h period ending at $t_c - 6$ h. The position of the front and the axis of maximum cyclonic relative vorticity at $t = 5.25$ days are indicated respectively by the solid and dashed lines.

gated by Sanders. This was accomplished by evaluation of the vorticity equation, with the beta effect omitted:

$$\frac{d}{dt}\left(\frac{\partial v}{\partial x'}\right) = -\mathrm{Ro}\left[\mathrm{Ro}\left(\frac{\partial u}{\partial x'}\frac{\partial v}{\partial x'} + \frac{\partial w}{\partial x'}\frac{\partial v}{\partial z'}\right) + \frac{\partial u}{\partial x'}\right]. \quad (10)$$

The first two terms on the right side of (10), associated with 1) convergence and 2) vertical tilting, are

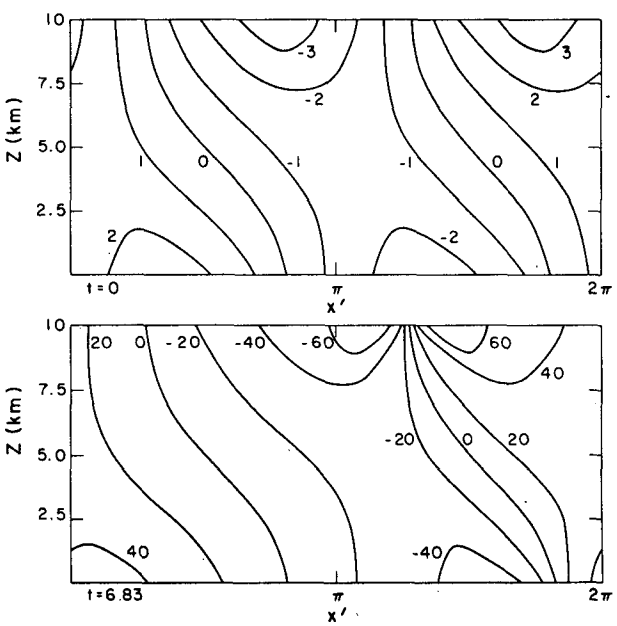

FIG. 9. Geostrophic flow v_g (m s^{-1}), with Ekman suction included in the model, at the initial time $t = 0$ and 6 h before the infinity in $\partial v_g/\partial x$ forms at the upper boundary, $t = 6.83$ days. The flow is cyclic over one wavelength of the disturbance, 2π, corresponding to $L = 4200$ km and the flow is stationary in the coordinate frame x' that moves at speed $\bar{u} + c_r$, where $\bar{u}$ is the midlevel translation speed and c_r the phase speed of the disturbance. $v_g = 0$ is coincident with the axis of maximum cyclonic relative vorticity $\partial v_g/\partial x'$.

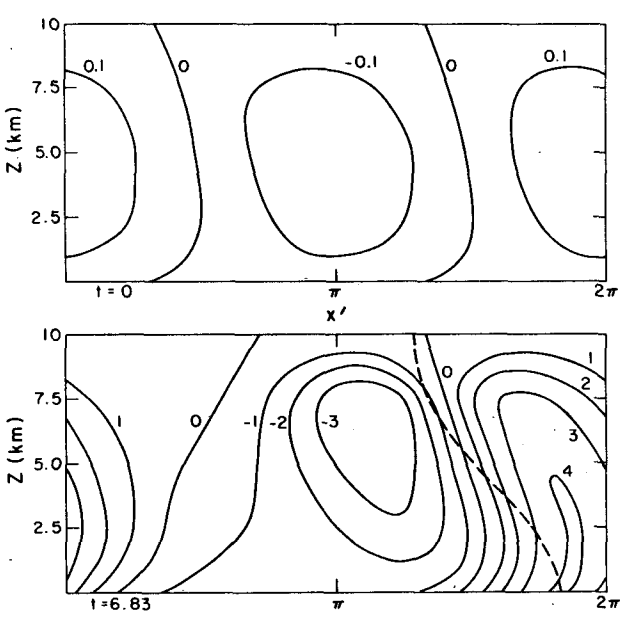

FIG. 10. As in Fig. 9, except for vertical velocity w (10^{-2} m s^{-1}). The dashed line represents the axis of maximum cyclonic relative vorticity.

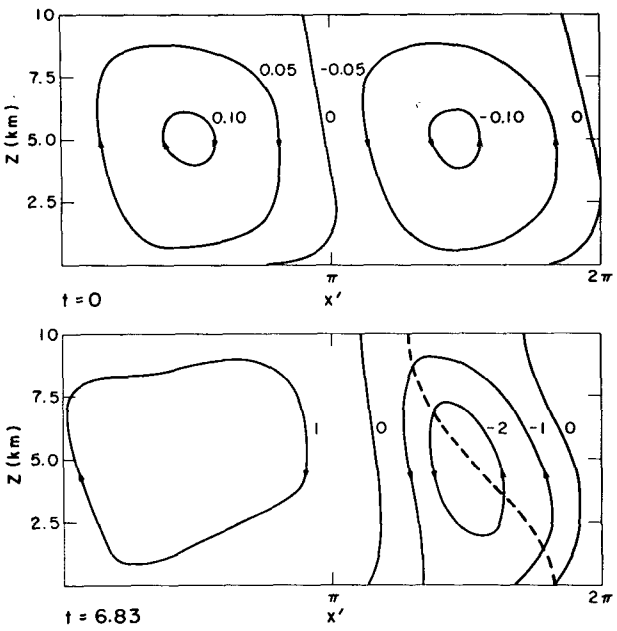

FIG. 11. As in Fig. 9, except for streamfunction of the ageostrophic motion field (10^4 m^2 s^{-1}).

analogous to the first two terms of (9); the third term is associated with the stretching of vortex lines by convergence.

Evaluation of each term in (10) appears in S(14), S(15) and S(16) respectively, while the net contribution is shown in S(17). The pattern of frontogenesis and frontolysis, contributed by the first two terms, resembles the pattern associated with the evaluation of (9). This circumstance arises because potential isotherms and isopleths of the wind component parallel to the front are essentially parallel to each other, particularly where the largest frontogenetical and frontolytical processes occur. Vortex stretching contributes to frontogenesis within the frontal zone but is otherwise negligible. The net contribution to (10) is again dominated by vertical tilting associated with the jet of vertical motion, while frontogenesis and frontolysis contributions from the individual terms tend to cancel within the frontal zone.

The evaluation of (10) by means of the HB model is shown in B(7a–7d). As before, the convergence term contributes to frontogenesis ahead of the front while tilting of v_g isopleths produces frontolysis at the upper portion of the frontal boundary. The similarity of this pattern to the results displayed in B(5a,5b) is also associated with parallelism between the potential isotherms and v_g isopleths that are shown in B(2,3). Vortex stretching [B(7c)] contributes little to (10), in agreement with Sanders' result. The net effect of these contributions shows that frontogenesis in the wind field occurs ahead of the front and is confined to the lowest kilometer above the ground. The magnitudes are about an order of magnitude smaller than those found by Sanders, principally due to the absence of the vertical motion jet near the axis of maximum cyclonic vorticity.

d. Trajectories

Trajectories of the air motion were computed at increments of 0.5 h for the 12 h period ending at $t_c - 6$ h. These trajectories are shown in B(8). In this coordinate frame, moving with the midlevel flow, the axis of maximum cyclonic vorticity remains essentially stationary. The ageostrophic mo-

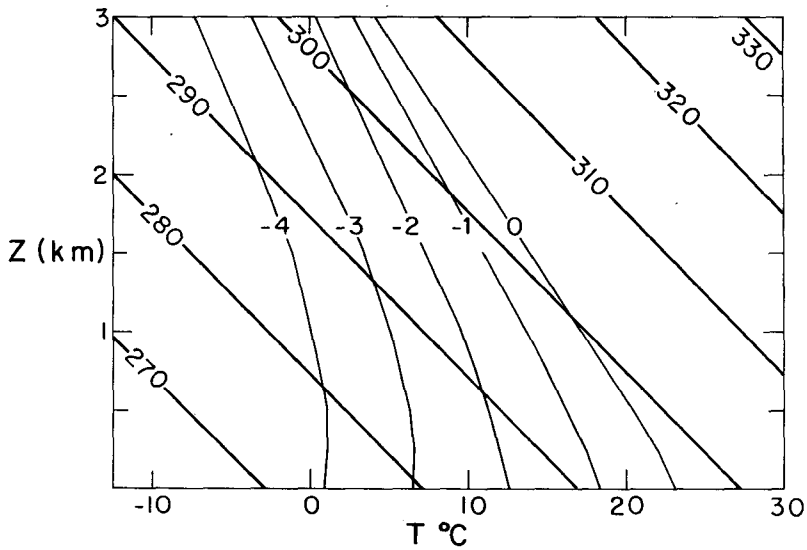

FIG. 12. Vertical distribution of temperature at $t = 6.83$ days, as in Fig. 1, with Ekman suction included in the model.

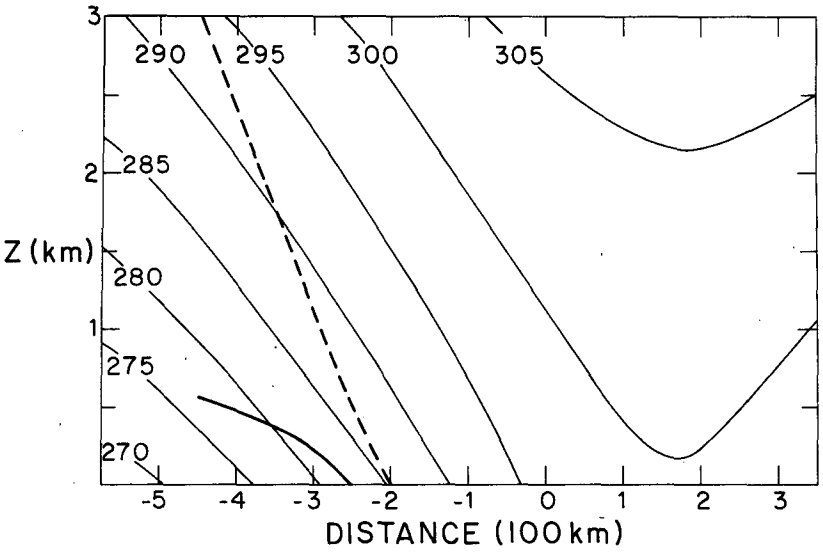

FIG. 13. Potential temperature (basic state and disturbance) distribution (K). Horizontal distance is measured from the point of maximum cyclonic relative vorticity at ground level. The front, determined from Fig. 12, is delineated by the thick solid line and the axis of maximum potential temperature gradient is shown by the dashed line.

tion that concentrates the cyclonic vorticity is superposed on a steady geostrophic translation, that moves from right to left in the cross section displayed. It is not until this late stage of growth, $t \approx t_c - 6$ h, that the velocity amplitude of the ageostrophic component u exceeds the translation speed at low levels.

Air tends to move westward relative to the mid-level zonal flow toward the front from the warm sector. It rises in response to the thermally direct circulation centered around the axis of maximum cyclonic vorticity (see Blumen, 1979, Fig. 5) and then continues to move westward aloft, circumventing the low-level frontal boundary. Air which was present between the ground and frontal surface 12 h earlier tends to remain here, since the positively directed ageostrophic horizontal component opposes and essentially balances the geostrophic translation.[2] There is some "entrainment" through the front, but for practical purposes it appears to be relatively small. In fact, these air trajectories provide an explanation for the vertical temperature distribution shown in B(1). Air in the warm sector of the wave moves toward the axis of maximum cyclonic vorticity, conserving its initial potential temperature. Upward motion then carries this relatively warm air aloft. In contrast, the air in the cold sector remains confined there, also conserving its relatively low potential temperature. This sequence of events leads to the succession of inversions which were used to define the front itself. In this sense, the front tends to appear as a substantial surface separating cold and warm air.

[2] This balance would not continue at later times, but then model predictions are not physically realistic.

4. Frontogenesis with the incorporation of an Ekman boundary layer

The absence of a rising jet in the HB model may be alleviated by incorporating Ekman suction as a parameterization of boundary layer processes. This parameterization produces upward motion through a cyclonic vortex. The mathematical aspects of the HB model solution with this added feature have been relegated to the Appendix. The geostrophic flow, vertical velocity and streamlines of the ageostrophic motion are displayed, respectively, in B(9,10,11) over one wavelength of the disturbance and throughout the total depth of the fluid. Two principal features of the motion, not present earlier, are 1) a rising jet that emanates from the boundary layer in association with cyclonic vorticity, $\partial v_g/\partial x' > 0$, and a broad, but relatively intense, downward flow in the anticyclonic region, $\partial v_g/\partial x' < 0$ and 2) the infinity in $\partial v_g/\partial x'$ that first forms on the upper boundary. This latter feature occurs because divergent outflow above the boundary layer ($z = 0$), evident in the streamfield [B(11)], reduces the intensity of frontogenesis. This latter effect is not prominent at the upper boundary.

The frontal boundary was determined, as before, with the aid of the model produced vertical temperature distribution in B(12). If the top of a low-level inversion or isothermal layer is used for this depiction, the front intersects the lower boundary ~250 km behind the axis of maximum cyclonic shear and

also behind the axis of maximum potential temperature gradient in B(13). These differences are even more pronounced than in the previous situation, displayed in B(2,3), and to the observed character of the front shown in S(9).

The trajectories associated with the incorporation of an Ekman layer (not shown) all tend to move generally upward and to the left in the lower layer frontal region. This behavior occurs because the magnitude of the ageostrophic horizontal velocity component u is smaller than the opposing geostrophic translation speed. As a consequence, some relatively warm air ahead of the axis of maximum cyclonic vorticity tends to move into the lower layers behind this axis, thus reducing the strength of the inversions displayed in B(12).

Evaluation of each term in (9) was carried out using the HB model-Ekman solution given in the Appendix. The sum of the convergence and vertical tilting terms are shown in B(14a). This figure essentially reflects the contribution from the convergence of potential isotherms. The vertical tilting term yielded a negligibly small contribution despite the existence of the relatively sharp jet of vertical motion shown in B(10). However, this jet occurs in association with the extremely weak vertical gradients of potential temperature, shown in B(13).

The principal contribution to frontogenesis is again the third term that distorts potential isotherms in the horizontal plane. The net contribution from all three terms, shown in (14b), is dominated by the third term. The distribution of frontogenesis and

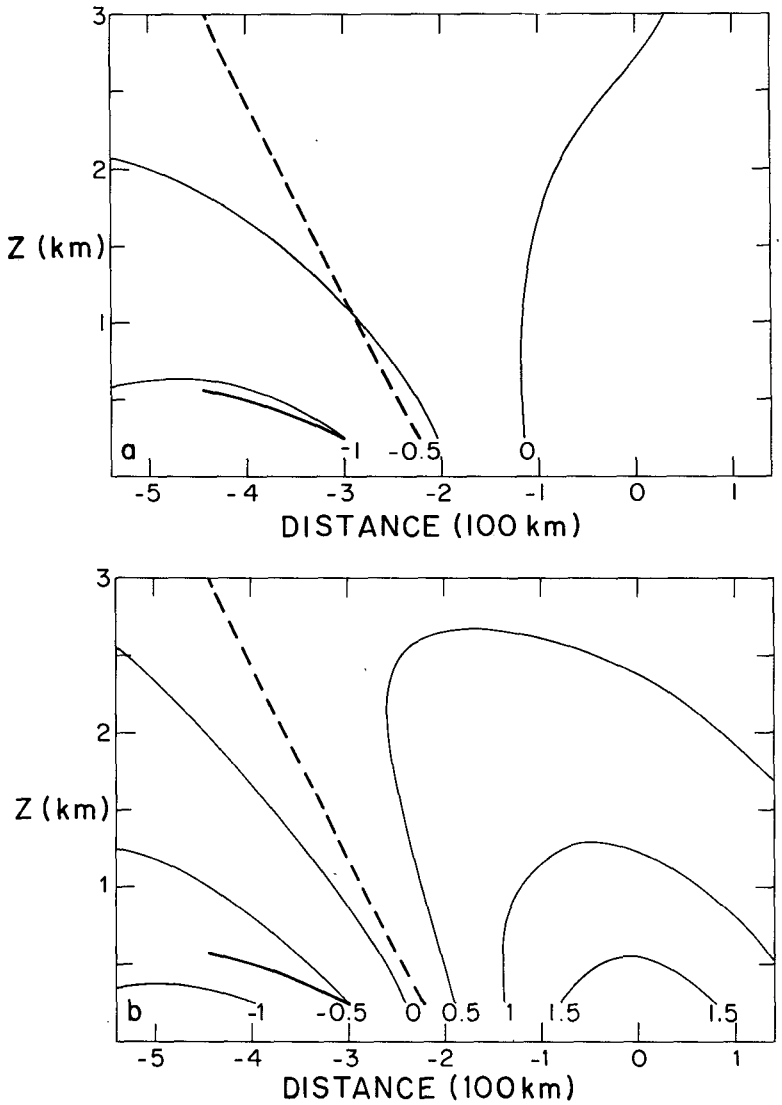

FIG. 14. Distribution of the frontogenetical effect, defined by (9), expressed in 3 h changes in the potential temperature gradient [K (100 km)$^{-1}$]: (a) $-\mathrm{Ro}^2\,\partial u/\partial x'\partial\theta/\partial x' - \mathrm{Ro}\,\partial w/\partial x'(1 + \mathrm{Ro}\,\partial\theta/\partial z')$ and (b) sum of all the contributions to (9), $-\mathrm{Ro}\,\partial v_g/\partial x' +$ (a).

frontolysis is similar to the field displayed in B(6b) but is of lesser intensity due to frontolytical properties associated with the inclusion of Ekman suction. Moreover, all contributions to the vorticity equation (10), not shown, are relatively small and inconclusive due to the weak gradients displayed by the present solution.

It is apparent that the Ekman boundary layer parameterization does not adequately model the low-level characteristics of the front. Convergence in the boundary layer should tend to concentrate gradients of wind and temperature while the divergent outflow aloft would be frontolytic. The present parameterization, in effect, only models this latter aspect of the flow.

5. Final remarks

In the present study, the Eady model of baroclinic instability and the physical features inherent in the one-dimensional advection equation (or the geostrophic coordinate transformation) provide a clear physical interpretation of the HB model of frontogenesis. This model exhibits relatively large-scale features that resemble the features displayed in analyses of atmospheric cold fronts. Sanders' (1955) case study of an intense cold front was examined to provide a more stringent test of the model.

On the basis of this comparison, the model appears to capture the essence of low-level frontogenesis for scales of motion as small as a few hundred kilometers. The basis for agreement is in the relative importance of physical processes and where they occur relative to the developing front. The model is not sufficiently realistic to provide quantitative verifications in the magnitudes of the computed frontogenetical properties or their small-scale spatial distribution, particularly in the frontal transition zone. Comparison was also limited by the apparent balance between frontolysis and frontogenesis in the analyzed front compared to the dominant frontogenetical properties of the model predictions. Moreover, the importance of latent heat release on frontogenesis remains an open question insofar as this study is concerned.

A major discrepancy between the model and analysis is the existence of a rising jet of air above the position of low-level maximum cyclonic vorticity in the analysis. As a consequence, the vertical tilting effect is the dominant frontogenetical feature of the analysis. It was possible to model the vertical velocity jet by incorporating Ekman boundary layer pumping into the model but, as explained in Section 4, the vertical tilting effect remained relatively small.

In conclusion, it appears that the HB model provides a useful prototype of low-level frontal development. Gradients of temperature and wind are intensified and energy cascades down the spectrum to smaller scales of motion from the initial energy-bearing baroclinic wave mode. However, the maximum intensities of these gradients do not coincide, so that the question of what constitutes a front or frontal zone has not been clarified by the model. Further understanding of low-level frontal formation will undoubtedly require the incorporation of latent heat release, a more realistic boundary-layer formulation, and a description of mesoscale mixing processes.

Acknowledgments. The numerical computations were carried out by K. Kanizay and financial support has been provided by the Atmospheric Research Section of the National Science Foundation under Grant ATM-7817615.

APPENDIX

Incorporation of Ekman Boundary-Layer Dynamics into the HB Model

Charney and Eliassen (1949) introduced a convenient parameterization of boundary layer dynamics by showing that the net mass transfer toward low pressure within an Ekman boundary layer produces a vertical velocity w at the top of this layer given by

$$w = \lambda\zeta, \tag{A1}$$

where ζ denotes the relative vorticity and, $\lambda = E^{1/2}/Ro$, where E denotes the Ekman number and Ro the Rossby number. Although this type of parameterization has been shown to be formally consistent within the constraints of quasi-geostrophic theory (e.g., Pedlosky, 1971), a similar development within the constraints of the geostrophic momentum approximation, that leads to the HB model, has not been carried out. This parameterization encompasses the physical process that produces upward motion through the boundary layer in regions of cyclonic vorticity and downward flow in anticyclones. Consequently, (A1) will be adapted simply as a parameterization in the present case. Although this step lacks a formal development, the use of (A1) does not lead to any violation of the conservation principles of the geostrophic momentum approximation, presented by Hoskins (1975), and uniform potential vorticity is maintained by the interior flow. Moreover, since λ is an adjustable parameter any neglected physical aspects of the boundary layer may, as a first approximation, be absorbed in the specification of numerical values of this parameter.

For the present purposes,[3] $\zeta = \partial v/\partial x \approx \partial v_g/\partial x$, where x is the space coordinate introduced in (1). The transformation to (X, Z, T) coordinates yields

[3] The neglected ageostrophic component of v for this model was shown by Blumen (1979) to be $O(Ro^2) < 10^{-1}$ compared to v_g.

$$w(X,Z,T) = \lambda(\partial^2\Phi/\partial X^2)/(1 - \mathrm{Ro}\ \partial^2\Phi/\partial X^2), \quad \text{(A2)}$$

where $\Phi(X,Z,T)$ is the geostrophic streamfunction $v_g = \partial\Phi/\partial X$. The streamfunction satisfies

$$(\partial^2/\partial X^2 + \partial^2/\partial Z^2)\Phi = 0 \quad \text{(A3)}$$

and the lower boundary condition is derived from

$$\left(\frac{\partial}{\partial T} + \bar{u}\frac{\partial}{\partial X}\right)\frac{\partial\Phi}{\partial Z} - \frac{\partial\Phi}{\partial X} + w\left(1 + \mathrm{Ro}\frac{\partial^2\Phi}{\partial Z^2}\right) = 0, \quad \text{(A4)}$$

which expresses conservation of potential temperature.

If (A3) is used to eliminate $\partial^2\Phi/\partial Z^2$ and (A2) is used to evaluate (A4) at the lower boundary, the boundary condition becomes

$$\left(\frac{\partial}{\partial T} + \bar{u}\frac{\partial}{\partial X}\right)\frac{\partial\Phi}{\partial Z} - \frac{\partial\Phi}{\partial X} + \lambda\frac{\partial^2\Phi}{\partial X^2} = 0, \quad Z = 0. \quad \text{(A5)}$$

The condition $w = 0$ is retained at the upper boundary ($Z = 1$). The mathematical problem is identical to the two-dimensional quasi-geostrophic Eady problem in physical space with Ekman pumping at the lower boundary. The eigenvalue problem has been solved by Hide (1969), Fischer *et al.* (1973) and Williams and Robinson (1974).

The solution may be expressed as in (2), but $X' = X - (\bar{u} + c_r)T = X - (\tfrac{1}{2} + c_r)T$, where c_r denotes the phase speed of the wave. The relevant parameters, representing the fastest growing wave disturbance, for $\lambda = 0.1$, are listed below:

growth rate: $\sigma = 0.23832$

phase speed: $c_r = -0.02668$

wavenumber: $k = 1.5$

$$A = 0.05\left[\left(\frac{b}{a}\right)^2 \sinh kZ' + \left(\cosh kZ' + \frac{d}{a}\sinh kZ'\right)^2\right]^{1/2}$$

$$\tan\delta = (b/a)/(\coth kZ' + d/a)$$

$$b/a = 1.76,$$

$$d/a = 0.50864.$$

These expressions reduce formally to those of the Eady model, with $w = 0$ at the lower boundary, when $\lambda = 0$, $d/a = 0$, and $(\sigma,k,b/a)$ assume their appropriate values (Blumen, 1979).

The infinity in $\partial v_g/\partial x'$ first forms at the upper boundary at the critical time $t_c = 7.08$ days for the parameter values used. The delay, compared to the previous case, is caused by the smaller growth rate in this case. The delay becomes greater for $\lambda > 0.1$, reaching 9 days for $\lambda = 0.2$. The computations presented in Section 4 represent the fields at $t_c - 6$ h as in the Section 3 presentation.

REFERENCES

Andrews, D. G., and B. J. Hoskins, 1978: Energy spectra predicted by semi-geostrophic theories of frontogenesis. *J. Atmos. Sci.*, **35**, 509–512.

Benton, E. R., and G. W. Platzman, 1972: A table of solutions of the one-dimensional Burgers equation. *Quart. Appl. Math.*, **30**, 195–212.

Blumen, W., 1979: Unstable nonlinear evolution of an Eady wave in time-dependent basic flows and frontogenesis. *J. Atmos. Sci.*, **36**, 3–11.

Bretherton, F. P., 1966: Baroclinic instability and the short wavelength cut-off in terms of potential vorticity. *Quart. J. Roy. Meteor. Soc.*, **92**, 335–345.

Charney, J. G., 1971: Geostrophic turbulence. *J. Atmos. Sci.*, **28**, 1087–1095.

——, and A. Eliassen, 1949: A numerical method for predicting the perturbations of the middle latitude westerlies. *Tellus*, **1**, 38–54.

Fischer, G., E. Heise and V. Renner, 1973: The effect of surface friction on the development of cyclone waves in a numerical model. *Beitr. Phys. Atmos.*, **46**, 157–181.

Fubini-Ghiron, E., 1935: Anomalie nella propagazione di onde acustiche di grande ampiezza. *Alta Frequenza*, **4**, 530–581.

Gall, G., R. Blakeslee and R. C. J. Sommerville, 1979: Baroclinic instability and the selection of the zonal scale of the transient eddies of middle latitudes. *J. Atmos. Sci.*, **36**, 767–784.

Hide, R., 1969: Some laboratory experiments on free thermal convection in a rotating fluid subject to a horizontal temperature gradient and their relation to the theory of the global atmosphere circulation. *The Global Circulation of the Atmosphere*, G. A. Corby, Ed., Roy. Meteor. Soc., 196–221.

Hoskins, B. J., 1975: The geostrophic momentum approximation and the semi-geostrophic equations. *J. Atmos. Sci.*, **32**, 233–242.

——, 1976: Baroclinic waves and frontogenesis. Part I: Introduction and Eady waves. *Quart. J. Roy. Meteor. Soc.*, **102**, 103–122.

——, and F. P. Bretherton, 1972: Atmospheric frontogenesis models: Mathematical formulation and solution. *J. Atmos. Sci.*, **29**, 11–37.

——, and N. V. West, 1979: Baroclinic waves and frontogenesis: Part II. Uniform potential vorticity jet flow—cold and warm fronts. *J. Atmos. Sci.*, **36**, 1663–1680.

Miller, J. E., 1948: On the concept of frontogenesis. *J. Meteor.*, **5**, 169–171.

Pedlosky, J., 1971: Geophysical fluid dynamics, mathematical problems in the geophysical sciences. *Lectures in Applied Mathematics*, Vol. 13, Amer. Math. Soc., 1–60.

Platzman, G. W., 1964: An exact integral of complete spectral equations for unsteady one-dimensional flow. *Tellus*, **16**, 422–431.

Sanders, F., 1955: An investigation of the structure and dynamics of an intense surface frontal zone. *J. Meteor.*, **12**, 542–552.

Williams, G. P., and J. B. Robinson, 1974: Generalized Eady waves and Ekman pumping. *J. Atmos. Sci.*, **31**, 1768–1776.